The Chittagong Univ. J. Sci. 46(1): 137-163, 2025

In Silico Identification of Potent SARS-CoV-2 RdRp Inhibitors: DFT and Molecular Docking Analysis of Acylated Glucopyranoside Derivatives

Sarkar M. A. Kawsar*, Md. Rithoan Hossain, Niloy Bhattacharjee, Nasrin S. Munia, Jannatul Ferdous, and Mariam Islam

Lab of Carbohydrate and Nucleoside Chemistry (LCNC), Department of Chemistry, Faculty of Science, University of Chittagong, Chittagong-4331, Bangladesh

**Corresponding author: akawsar@cu.ac.bd*

Manuscript received on 16/11/2025, Revised manuscript received on 30/12/2025, and accepted on 30/12/2025.

Abstract

Severe acute respiratory syndrome (SARS) is a global health threat caused by severe acute respiratory syndrome coronavirus 2 (SARS-CoV-2), highlighting the urgent need for the development of new therapeutic agents. This study involves a computational investigation of the design and assessment of several methyl α-D-glucopyranoside (MDG) derivatives as potential inhibitors of the SARS-CoV-2 RdRp chain. MDG derivatives **2-5** were optimized through quantum mechanical methods, and their therapeutic potential properties against SARS-CoV-2 was evaluated through a comprehensive in silico approach. Thermodynamic properties and frontier molecular orbital (FMO) studies were utilized to characterize the chemical stability and reactivity. Molecular electrostatic potential (MEP) and natural bond orbital (NBO) charge analyses revealed the reactive electrophilic and nucleophilic sites within the derivatives. Molecular docking was employed to predict the binding affinities and interaction profiles of the SARS-CoV-2 RdRp chain targets (PDB ID: 6M71). Molecular docking simulations indicated that compound **2**, with its long aliphatic chains, exhibited the highest binding affinity, with a docking score of -7.1. The strong hydrogen bonding interactions with LYS47 and HIS133 and one hydrophobic contact with ALA130 (5.20 A), a key residue involved in active site accessibility, contributed to the high binding affinity of compound **2**. Additionally, LYS47 formed strong hydrogen bonds with the derivative. ADMET predictions suggested that the derivatives generally possess a favorable safety profile, with low genotoxicity and neurotoxicity. Overall, these results demonstrate the promise of modified MDG derivatives as lead compounds and justify further *in vitro* and *in vivo* studies to validate their antiviral activity against SARS-CoV-2.

Keywords: *Glucopyranoside; SARS-CoV-2 RdRp; DFT; Molecular docking; ADMET*

DOI: https://doi.org/10.3329/cujs.v46i1.90724

সারমর্ম: তীব্র আচম্বিত শ্বাসযন্ত্রের সংক্রমণ সিন্ড্রোম (SARS) একটি মারাত্মক বৈশ্বিক স্বাস্থ্যঝুঁকি হিসেবে বিবেচিত, যা SARS-CoV-2 দ্বারা সৃষ্ট এবং এর মোকাবিলায় নতুন চিকিৎসা উপকরণ উদ্ভাবনের তাৎক্ষণিক প্রয়োজনীয়তা তুলে ধরে। এই গবেষণায় কম্পিউটেশনাল পদ্ধতির মাধ্যমে কিছু মিথাইল α-D-গ্লুকোপাইরানোসাইড (MDG) জাতকের নকশা ও মূল্যায়নকে SARS-CoV-2 RdRp চেইনের সম্ভাব্য অবদমনকারী হিসেবে অনুসন্ধান করা হয়েছে। MDG

জাতক ২-৫ কে কোয়ান্টাম মেকানিক্যাল পদ্ধতিতে অপ্টিমাইজ করা হয়েছে এবং SARS-CoV-2-এর বিরুদ্ধে তাদের চিকিৎসাগত সম্ভাবনাকে একটি সমন্বিত ইন সিলিকো পদ্ধতির মাধ্যমে মূল্যায়ন করা হয়েছে। তাপগতীয় বৈশিষ্ট্য এবং ফ্রন্টিয়ার আণবিক অরবিটাল (FMO) বিশ্লেষণের মাধ্যমে রাসায়নিক স্থিতিশীলতা ও বিক্রিয়াশীলতা নির্ধারণ করা হয়েছে। আণবিক ইলেক্ট্রোস্ট্যাটিক পটেনশিয়াল (MEP) এবং প্রাকৃতিক বন্ধন অরবিটাল (NBO) চার্জ বিশ্লেষণ দ্বারা জাতকগুলির অভ্যন্তরে বিক্রিয়াশীল ইলেক্ট্রোফিলিক ও নিউক্লিওফিলিক সাইটগুলো শনাক্ত করা হয়েছে। মলিকুলার ডকিং ব্যবহার করে SARS-CoV-2 RdRp চেইনের টার্গেট (PDB ID: 6M71)-এর সাথে তাদের বন্ধন প্রবণতা ও প্রতিক্রিয়া বৈশিষ্ট্য এর পূর্বাভাস দেওয়া হয়েছে। মলিকুলার ডকিং সিমুলেশন নির্দেশ করে যে জাতক ২, যার দীর্ঘ আলিফ্যাটিক শৃঙ্খল (প্যালমিটয়ল গ্রুপ) রয়েছে, সবচেয়ে উচ্চ সংযুক্তি প্রবণতা প্রদর্শন করেছে যার ডকিং স্কোর -৭.১। LYS47 এবং HIS133-এর সঙ্গে শক্তিশালী হাইড্রোজেন বন্ধন আন্তঃক্রিয়া এবং ALA130 (5.20 Å)-এর সঙ্গে একটি হাইড্রোফোবিক সংযোগ স্থাপন, যা সক্রিয় স্থানে প্রবেশযোগ্যতায় গুরুত্বপূর্ণ ভূমিকা রাখে, যা জাতক ২-এর উচ্চ বন্ধনের আকর্ষণ ক্ষমতায় অবদান রেখেছে। এছাড়াও, LYS47 জাতকটির সঙ্গে শক্তিশালী হাইড্রোজেন বন্ধন গঠন করেছে। ADMET বিশ্লেষণে প্রতীয়মান হয়েছে যে উল্লিখিত যৌগসমূহ সামগ্রিকভাবে অনুকূল নিরাপত্তা প্রোফাইল প্রদর্শন করে, এবং জিনগত ও স্নায়ুতন্ত্রসংক্রান্ত বিষাক্ততা তুলনামূলকভাবে কম। এ ফলাফলগুলো পরিবর্তিত MDG জাতকসমূহকে সম্ভাবনাময় মুখ্য যৌগ হিসেবে প্রদর্শন করে এবং SARS-CoV-2-এর বিরুদ্ধে তাদের ভাইরাসবিরোধী কার্যকারিতা নিরূপণের জন্য আরও in vitro ও in vivo গবেষণার প্রয়োজনীয়তাকে জোরালোভাবে নির্দেশ করে।

Abbreviations

ADMET: Absorption, distribution, metabolism, excretion, and toxicity

DFT: Density functional theory

HOMO: Highest occupied molecular orbital

LUMO: Lowest unoccupied molecular orbital

MEP: Molecular electrostatic potential

NBO: Natural bond orbital

SARS-CoV-2: Severe acute respiratory syndrome coronavirus 2

1. Introduction

The extremely contagious and dangerous severe acute respiratory syndrome coronavirus 2 (SARS-CoV-2) (Figure 1), the primary cause of the COVID-19 pandemic, has disseminated quickly and presented an unparalleled health hazard to the global population. The novel SARS-CoV-2 was initially reported in December 2019 to have originated in the live animal market in Wuhan, Hubei Province, where it has induced pneumonia-like respiratory infections in the local human population [1,2]. Although vaccines and promising therapies have been developed for SARS-CoV-2, the pursuit of novel drug development remains a priority because of the continuous worldwide health threats caused by COVID-19 [3].

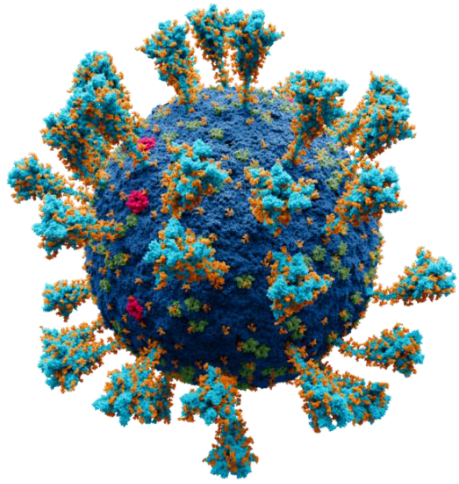

Figure 1. Atomic model of the external structure of SARS-CoV-2 [source: Wikipedia].

A common class of essential macromolecules present in all living organisms is carbohydrates. Numerous essential biological functions, including cellular proliferation, intercellular signaling, and immunological responses are performed by living organisms. Moreover, they demonstrate considerable biological efficacy against many pathogens and offer therapeutic benefits for other disorders. A thorough examination of the current literature indicates that numerous biologically active molecules possess aromatic, heteroaromatic, and acyl substituents [4–7]. Compounds such as benzene, its substituted derivatives, and those containing heteroatoms and halogens are recognized for their ability to increase the biological efficacy of their parent molecules [8,9]. The introduction of an active substituent into an inactive molecule is expected to enhance its potential biological function [10]. Furthermore, the targeted acylation of carbohydrates, along with microbial activity assessments [11,12], has revealed that, in multiple instances, the synergistic effect of combining two or more heteroaromatic scaffolds with acyl groups markedly improves biological activity relative to the parent structure [13]. Monosaccharide esters exhibit a broad spectrum of antibacterial activity against gram-negative and gram-positive pathogens, such as *Escherichia coli*, *Bacillus subtilis*, *Salmonella typhi*, and *Staphylococcus aureus* [14]. In contrast, it has been demonstrated that altered hydroxyl (-OH) groups in nucleoside and monosaccharide structures possess unique and powerful antibacterial and antiviral characteristics [15,16].

Glycans, a distinct class of carbohydrates, are implicated in a variety of disorders, including cancer, inflammation, and microbial infections. Leveraging the specific interactions between glycans and lectins has facilitated significant progress in vaccine development, antiviral therapeutics, and immunotherapies [17,18]. Recently, advanced techniques have been employed to isolate diverse natural products from plants [19] and other sources, many of which contain carbohydrates as key constituents exhibiting cytotoxic activity [20].

Among the most accessible and effective targets for antiviral drug design is the RNA-dependent RNA polymerase (RdRp) of SARS-CoV-2, which plays a central role in viral replication and transcription of the RNA genome. Unlike host polymerases, RdRp lacks a direct human homolog, reducing the risk of off-target effects and making it an attractive target for inhibitors. The catalytic domain of the enzyme is highly conserved and forms the core of viral RNA synthesis, with nucleotide incorporation occurring in a template-dependent manner; its inhibition effectively halts viral replication [21,22]. Several clinically approved antiviral drugs, including remdesivir, target this polymerase, further underscoring its pharmacological significance. Thus, RdRp (PDB ID: 6M71) was selected as the molecular target for the current study to identify potential inhibitors capable of interacting with its active site residues and disrupting viral replication [23]. RdRp represents a highly conserved and essential therapeutic target due to its pivotal role in viral RNA replication, protein translation, and viral maturation [24]. Inhibition of this enzyme effectively interferes with the viral life cycle and suppresses disease progression. The present in silico study was conducted to evaluate the antiviral properties of MDG derivatives (**2-5**), with a particular focus on SARS-CoV-2 inhibition. Specifically, the inhibitory potential of these compounds against the SARS-CoV-2 RdRp crystal structure was assessed as a strategic approach to identify effective antiviral agents. Notably, the strong binding affinity of compound **2** indicates its potential as a potent RdRp inhibitor.

DFT analyses, encompassing reactivity descriptors, partial charges, and MEP maps, identified the reactive sites and potential interaction regions within the compounds. Furthermore, ADMET predictions revealed that these compounds exhibit favorable pharmacokinetic and safety profiles, supporting their potential as therapeutic agents. Given these promising characteristics, the compounds warrant further investigation through comprehensive *in vitro* and *in vivo* studies. In the present study, a series of MDG derivatives (**2–5**) were selected due to their distinctive structural features and potential biological activities [25]. Coronaviruses are infectious pathogens that primarily cause respiratory and intestinal infections. Given the urgent need for novel therapies, computational approaches provide a rapid and cost-effective means of identifying potential drug candidates. This strategy focuses on key viral proteins that are essential for the replication and survival of SARS-CoV-2.

Carbohydrate-based drugs, such as remdesivir, which incorporates a ribose moiety, have demonstrated high efficacy and are considered promising treatments for COVID-19 in both previously treated and untreated patients (Figure 2).

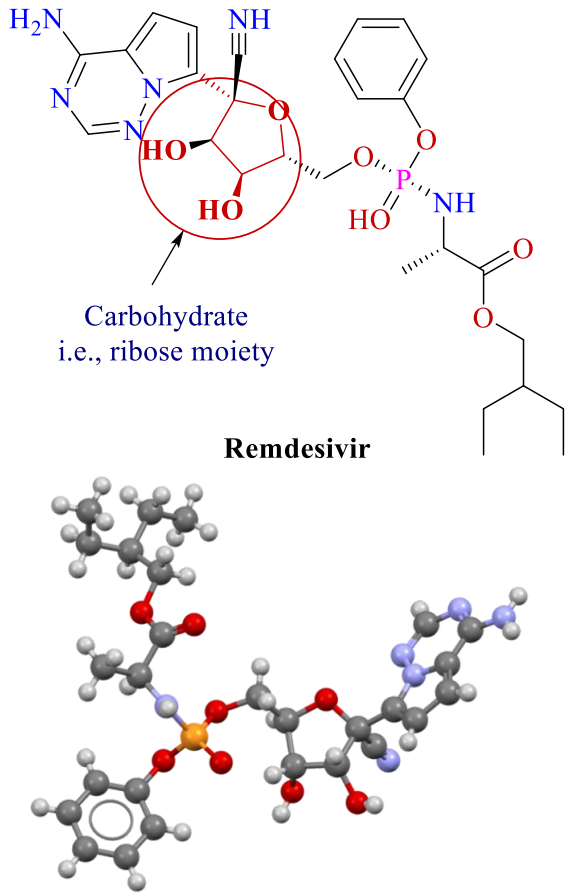

Figure 2. Marketed SARS-CoV-2 remdesivir drugs with carbohydrate moieties. (*Left*: 2D structure and *right*: 3D structure of the remdesivir).

Figure 3 presents a detailed flow diagram of the research process, outlining the sequential steps, methodologies, and key components.

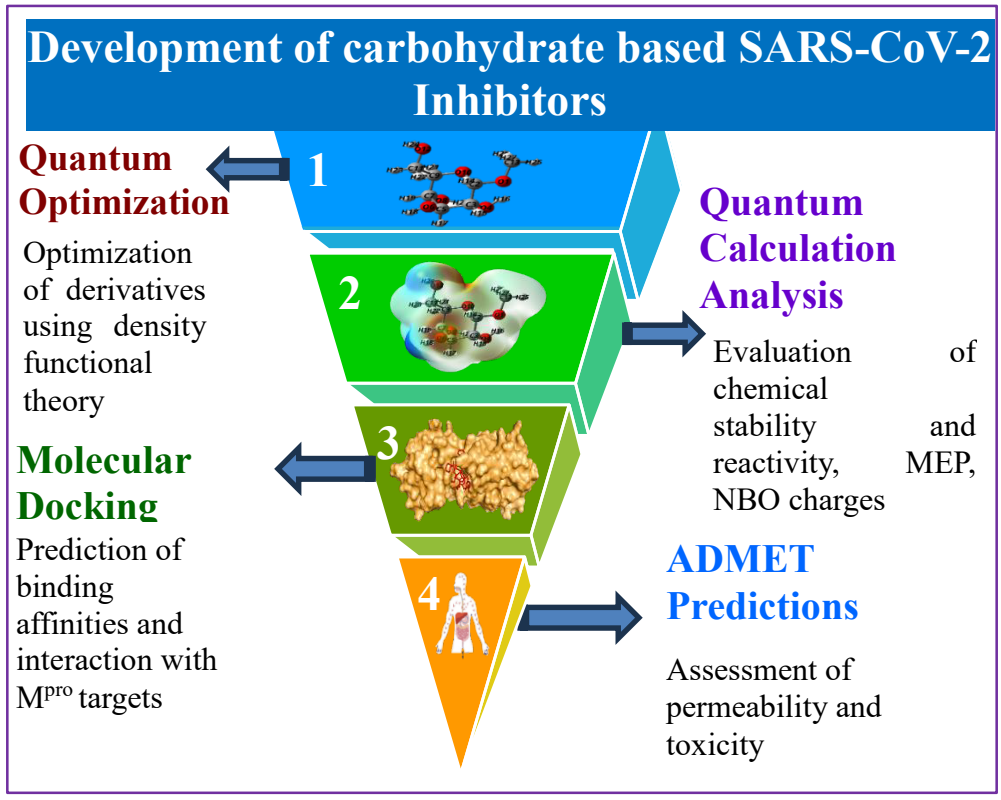

Figure 3. Current research study workflow diagram: sequential steps and key elements.

2. Materials and Methods

2.1 Reactivity and electronic structure calculations

DFT approach was employed to calculate the optimized geometries, electronic properties, and reactivity parameters of the studied compounds, providing insights into their structural stability, reactive sites, and potential intermolecular interactions. The 2D and 3D optimized structures of the studied compounds are presented in Table 1.

Table 1. 2D- and 3D-optimized structures of the studied methyl α-D-glucopyranoside (**1**) and its analogs (**2-5**) and the substituents of the analogs.

Entry	2D structures	3D structures
1	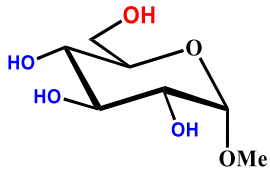	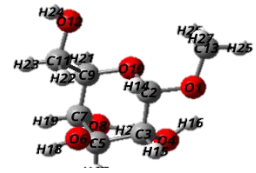
2	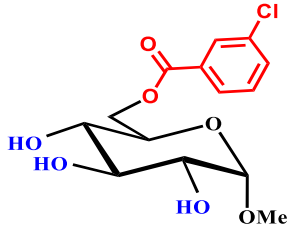	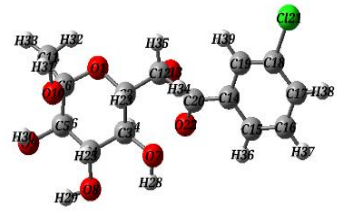
3	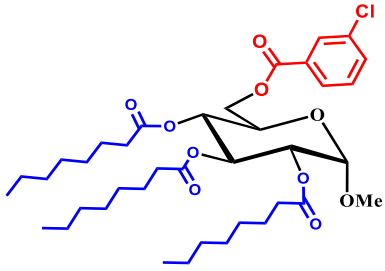	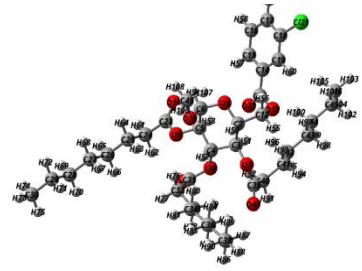
4	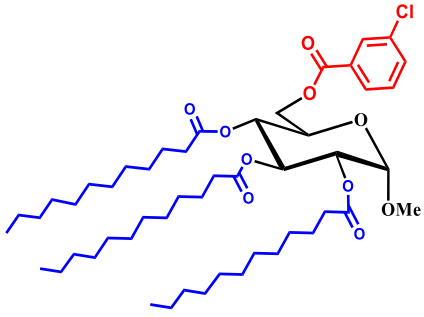	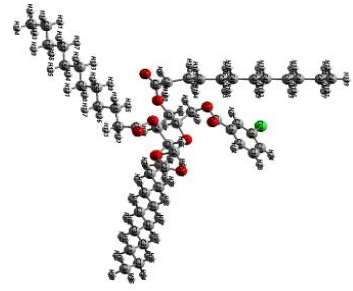

5

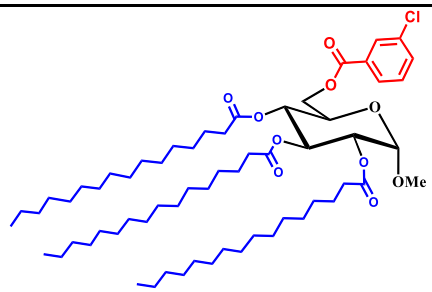

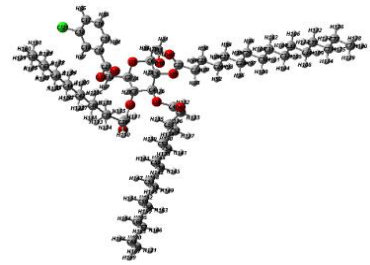

The chemical properties were determined via the Gaussian 09 W software suite [26]. Following the optimization process, GaussView 6.0 [26] displayed the molecular geometries. This enabled the examination of the optimized structures and the investigation of various molecular features. The geometry was optimized with the B3LYP exchange functional developed by Becke [27], which incorporates the LYP correction [28], along with the 3-21G basis set. Molecular electrostatic potential (MEP) maps were generated via GaussView 6.0 to depict the distribution of electrostatic potential across the molecular structures. The reactivity and electronic structural features were assessed through the energies of the lowest unoccupied molecular orbital (LUMO), the highest occupied molecular orbital (HOMO), the energy gap, the chemical potential (μ), the chemical hardness (η), electronegativity (χ), and the global electrophilicity (ω). The values of these variables were calculated via the following formulas on the basis of the HOMO and LUMO energies [29].

$$\text{Energy Gap } (\Delta\varepsilon) = [\varepsilon\text{LUMO} - \varepsilon\text{HOMO}]$$

$$\eta = \frac{[\varepsilon\text{LUMO} - \varepsilon\text{HOMO}]}{2}$$

$$S = \frac{1}{\eta}$$

$$\mu = \frac{[\varepsilon\text{LUMO} + \varepsilon\text{HOMO}]}{2}$$

$$\chi = -\frac{[\varepsilon\text{LUMO} + \varepsilon\text{HOMO}]}{2}$$

$$\omega = \frac{\mu^2}{2\eta}$$

2.2 Molecular docking studies

Methyl-α-D-glucopyranoside was molecularly docked to the RNA-dependent RNA polymerase (RdRp) of SARS-CoV-2 (PDB ID: 6M71) to examine its possible

inhibitory effect on viral replication [30]. RdRp was obtained in 3D crystal form from the RCSB Protein Data Bank and prepared by removing water molecules, co-crystalized ligands, and nonessential heteroatoms to create a pure binding environment. Polar hydrogen was introduced, and energy minimization of the structure was performed to maximize the bond angles and eliminate steric strain. The ligand methyl-α-D-glucopyranoside was retrieved from the PubChem database, and its 3D structure was generated with the help of molecular modeling software. Geometric optimization of the compound under the MM2 force field was performed to establish a stable conformation that can be used to dock the compound. The selected active site residues of RdRp were the main catalytic amino acids ASP760, ASP761, and SER759, which were chosen because of their presence in the literature and structure. The docking simulations were performed with the help of AutoDock Vina [31,32], where a grid box was created around the catalytic site to cover all the possible binding pockets. The docking algorithm produced a set of multiple ligands poses ranked by their binding affinities (in kcal/mol), and the highest-scoring conformation was further assessed. PyMOL and BIOVIA Discovery Studio Visualizers were used to visualize and analyze the docked complex to determine the presence of hydrogen bonding, hydrophobic contacts, and other noncovalent interactions that lead to complex stability. The distances of the most important interactions were measured to determine how the methyl-α-D-glucopyranoside inserts and stabilizes in the active pocket of the RdRp.

2.3 ADMET prediction

Computational analyses were performed to assess the ADMET (absorption, distribution, metabolism, excretion, and toxicity) profiles of the synthesized compounds. These evaluations provided crucial insights into their pharmacokinetic properties, safety, and drug-likeness, helping to determine their potential suitability for advancement to preclinical studies. The SwissADME online web application (http://www.swissadme.ch/) was used to predict the physicochemical and drug-likeness properties [33]. For each derivative, we entered the canonical SMILES notation to find important parameters that affect oral bioavailability. These parameters were used to determine whether Lipinski's rule [34] of five was followed and to determine the bioavailability score (BA): molecular weight (Mol. Wt.), hydrogen bond acceptors (HBAs), hydrogen bond donors (HBDs), LogP/w (lipophilicity), number of rotatable bonds (NRBs), and total polar surface area (TPSA). Moreover, the ProTox-Tox 3.0 online web server (https://tox.charite.de /protox3/) was used to look at the preliminary safety and toxicity profiles. This server uses QSAR models to guess toxicity endpoints. This analysis specifically predicted several important organ toxicities (hepatotoxicity, nephrotoxicity, neurotoxicity, and cardiotoxicity) and genotoxicity endpoints (carcinogenicity, immunotoxicity,

mutagenicity, and cytotoxicity). It provides a binary prediction (Active/Inactive) and a confidence probability score for each compound.

3. Results and Discussion

3.1 Structural features of the MDG derivatives

The new analogs of methyl α-D-glucopyranoside used in this study were constructed according to the reaction scheme. The molecular docking assessment, supported by nonbonding interactions, hydrogen bonding, and hydrophobic surface analyses, confirmed that the activity of methyl α-D-glucopyranoside derivatives increases with an increasing number of hydrophobic chains [35].

3.2 Thermodynamic analysis

Typically, alterations in the molecular structure significantly influence the structural properties, including the thermal and molecular orbital parameters. The spontaneous reaction and stability of a product can be elucidated from the free energy and enthalpy values [36]. Highly negative values are more suitable for thermal stability. In drug design, hydrogen bond formation and nonbonded interactions are also influenced by the dipole moment. A higher dipole moment can improve the binding properties [6]. Using DFT calculations, the electronic energy, enthalpy, and Gibbs free energy were determined for the optimal geometries of the MDG derivatives (**2**-**5**). Table 2 shows that the electronic energy, which is the total energy without zero-point corrections, ranges from -722.215 Hartree for the parent compound (**1**) to -3620.104 Hartree for the largest derivative (**5**). The Gibbs free energy ranges from -721.807 Hartree (**1**) to -3620.035 Hartree (**5**). This association is anticipated, as larger, more atom-dense molecules exhibit markedly lower total energy relative to simpler structures, hence validating the thermodynamic stability of all produced derivatives in their optimal ground states. The dipole moment (measured in Debye, D) is very important for understanding how the electrostatic charge is spread out and how polar molecules are. This is a major aspect of how molecules interact with each other, the soluble nature they ought to have, and their ability to interact with biological targets. The parent molecule, MDG (**1**), has a dipole moment of 3.96 D. Interestingly, derivative **2** has a slightly lower value of 3.46 D. This is probably because it has a very symmetrical structure, which cancels out charges inside the molecule, even though it has a chlorine atom. The highly substituted derivatives **3**, **4**, and **5**, on the other hand, have the largest dipole moments. Compound **3** has the highest value at 5.90 D, and compounds **4** and **5** remain high at approximately 5.6 D. This significant change in polarity of the lead compounds is attributed to their highly uneven substitution pattern, particularly the incorporation of multiple 3-chlorobenzoyl groups and long aliphatic chains. These chains add highly polarizable heteroatoms (Cl and O) and change the electron density. These higher dipole moments imply that the altered

compounds may demonstrate improved capacity for advantageous electrostatic and hydrogen-bonding interactions with polar residues in the aqueous environment of the enzyme's active site, facilitating increased receptor binding and possibly increased solubility.

Table 2. Stoichiometry, electronic energy, enthalpy, Gibbs free energy in Hartrees, dipole moment (Debye), and polarizability (a.u.) of MDG derivatives (**2-5**).

Entry	Stoichiometry	Electronic Energy	Enthalpy	Gibbs Free Energy	Dipole Moment
1	$C_7H_{14}O_6$	-722.215	-721.753	-721.807	3.960989
2	$C_{14}H_{17}ClO_7$	-1522.367	-1521.872	-1522.192	3.464691
3	$C_{38}H_{59}ClO_{10}$	-2681.672	-2681.141	-2681.512	5.90347
4	$C_{50}H_{83}ClO_{10}$	-3150.888	-3150.248	-3150.406	5.609470
5	$C_{62}H_{107}ClO_{10}$	-3620.104	-3619.707	-3620.035	5.578195

3.3 Frontier molecular orbitals analysis

Table 3 shows how the intrinsic chemical stability and reactivity of the MDG derivatives (**2-5**) were measured by DFT descriptors.

Table 3. Energy (eV) of the HOMO, LUMO, energy gap, hardness, and softness of MDG and its derivatives (**2-5**).

Entry	HOMO	LUMO	Gap	Hardness	Softness
1	-6.09018	1.46125	7.55143	3.775715	0.264850
2	-6.95332	-0.34721	6.60611	3.303055	0.302750
3	-6.70216	-0.82586	5.87630	2.938150	0.340350
4	-6.61998	-0.74994	5.87004	2.935020	0.340713
5	-6.61536	-0.75103	5.86433	2.932165	0.341044

The energy of the highest occupied molecular orbital (HOMO) reflects how well a molecule can give up electrons, and the energy of the lowest unoccupied molecular orbital (LUMO) reflects how well it can take in electrons. When a molecule is modified, the HOMO energy usually decreases from parent molecule **1** (-6.09 eV) to its derivative. This makes the compounds more stable and suggests that they are less nucleophilic. On the other hand, the LUMO energy decreases substantially from 1.46

eV in compound **1** to negative values in the substituted compounds. This means that the compounds have become more electrophilic and are more likely to take up electrons. The energy gap (E_g), which is the difference between the LUMO and HOMO, is the most important indicator of chemical stability. A smaller gap means that the chemical is more reactive and less stable in motion. Compound **1** has the largest gap (E_g = 7.55 eV), which shows that it is quite stable. The modified derivatives (**2**-**5**), on the other hand, indicate a large decrease in the gap (down to 5.87 eV), which means that they are more reactive and less stable. The concepts of chemical hardness and softness further support this trend. The hardness of the substituted compounds decreases (from 3.78 to 2.93), and the softness increases (from 0.26 to 0.34). Compound **5** also had the lowest HOMO–LUMO gap and hardness, indicating that the molecule is more reactive than the other compounds are, according to Pearson *et al*. [29]. This finding shows that adding long-chain and aromatic groups makes the molecules chemically softer, more polarizable, and more reactive, which is beneficial for the occurrence of noncovalent interactions in a flexible enzyme binding pocket. The HOMO–LUMO diagrams of the compounds are displayed in Figure 4.

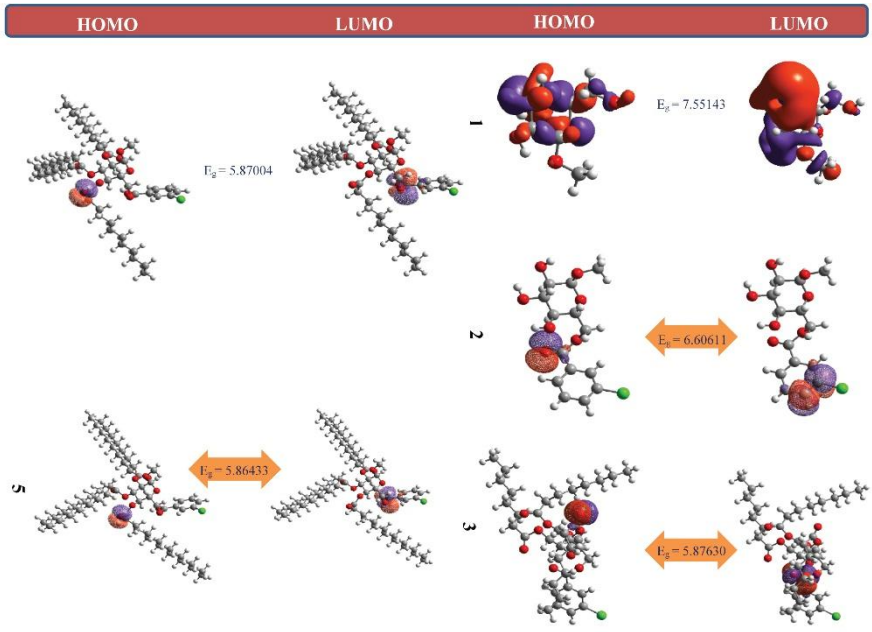

Figure 4. HOMO and LUMO distribution plots of the parent molecule MDG and its derivatives (**2**-**5**).

3.4 Molecular electrostatic potential

The molecular electrostatic potential (MEP) is widely used as a reactivity map displaying the most likely region for the electrophilic and nucleophilic attack of charged points, such as reagents, on organic molecules [37]. This method helps to interpret the biological recognition process and hydrogen bonding interactions [35]. This study was performed to illustrate the charge distribution throughout the molecular framework, offering a direct elucidation of the potential sites for electrostatic interactions and chemical reactivity. Most of the time, MEP maps use colors to represent areas with the highest negative potential (favored by electrophiles) in red and areas with the maximum positive potential (favored by nucleophiles) in blue. The green spots indicate that the potential is quite low. The MEP analysis of the MDG derivatives (**1**-**5**) clearly revealed that the areas with the most negative potential were the electronegative oxygen atoms of the sugar ring, the hydroxyl OH groups (in parent compound **1**), and, most importantly, the carbonyl (C=O) groups that were added by 3-chlorobenzoyl and long-chain substitutions in derivatives **2**-**5** (Figure 5). These negative areas are the most likely places where hydrogen-bond acceptors interact with important polar residues from biological targets. On the other hand, the largest positive potential is mostly around the hydrogen atoms on the outside, especially those that are attached to the ring carbons and the terminal hydrogens of the alkyl chains. These places give off hydrogen bonds. The addition of the chlorine atom to the aromatic ring in MDG derivatives (**2**-**5**) is very important because it produces a positive potential area surrounding the C-Cl bond, which slightly changes the electron density of the nearby aromatic system (Figure 5). The map shows that changing the glucopyranoside core strategically changed the electrostatic landscape.

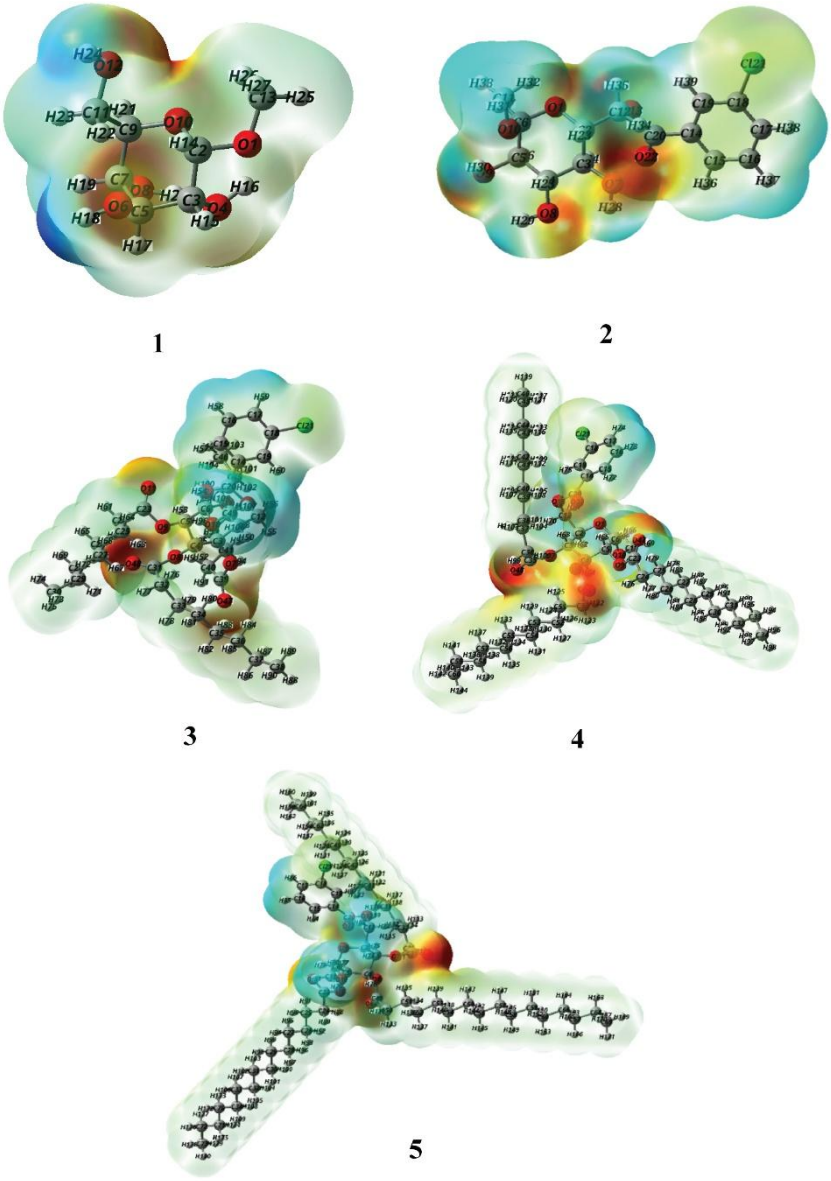

Figure 5. Molecular electrostatic potential map of MDG derivatives (**1**-**5**).

3.5 Atomic partial charges

The polarity of chemical bonds often dictates the structure and reactivity of a material [38,39]. A number of different methods have been proposed for assigning partial charges to the atoms of a molecule, including both quantum chemical and empirical schemes. Examining atomic partial charges using natural bond orbital (NBO) computations is important for determining the exact electrostatic forces that control ligand–receptor interactions. This information works well with the MEP and dipole moment data. The charge distribution is clearly defined when one looks at the molecular structures, such as those of compounds **2** and **4**. The most negative partial charges are always and clearly found on the highly electronegative oxygen atoms that make up the scaffold. These are the ring oxygens, the oxygens of any remaining hydroxyl groups (in parent structures), and most importantly, the carbonyl oxygens (C=O) that were added by substitutions. These sites with many electrons are the main hydrogen bond acceptors that may interact with polar residues in the M^{pro} pocket. On the other hand, the carbon atoms that are next to the oxygen atoms that pull electrons away from them have the highest positive partial charges. The carbonyl carbons such as C20, C23, C35, and C45 in compounds **3**, **4,** and **5** are the most electrophilic in nature because they bond with the highly electronegative element oxygen (Figure 6). Moreover, the hydrogen atoms that are linked to the carbon atoms of the glucopyranoside ring contain partial positive charges. These partial charges are very important since the strength of the electrostatic part of the binding free energy depends on how far apart they are. The most powerful MDG derivatives (**3**, **4**, and **5**) include many carbonyl and chloroaromatic groups, which makes the charge distribution quite uneven. This is what gives them high dipole moments.

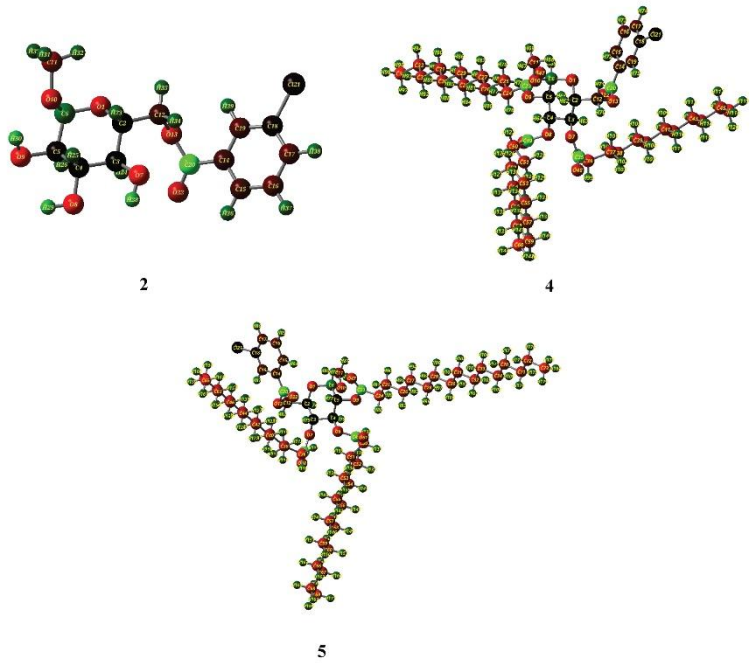

Figure 6. Atomic partial charges of MDG derivatives **2**, **4,** and **5**.

3.6 Molecular docking analysis

Owing to its essential and nonredundant role in cleaving viral polyproteins required for replication, SARS-CoV-2 RdRp has been conclusively identified as a key molecular target for the development of antiviral therapeutics against coronaviruses. Molecular docking simulations were performed against 6M71, which is very similar to the SARS-CoV-2 enzyme, to precisely evaluate the binding potential of the synthesized MDG derivatives (**2-5**). Because of this high degree of conservation, the geometry of the active pocket and the reported binding site residues are chemically important for predicting SARS-CoV-2 inhibition [40]. Molecular docking of the identified compounds with the main protease (6M71) indicated that the binding affinities of the identified compounds with the main protease ranged between -4.3 and -7.1 kcal/mol, and the reference compound Remdesivir had a much stronger binding affinity of -10.4 kcal/mol. Among the tested compounds, compounds **2** (-7.1 kcal/mol) and 4 (-6.5 kcal/mol) were the most favorable, which indicated greater inhibitory activity, as shown in Table 4 [41]. Complex stability was significantly affected by hydrogen bonding, and all the compounds were hydrogen bonded to active site residues (3-5 hydrogen bonds). Additionally, some ligands (especially

entries **3** and **4**) were found to have hydrophobic and π-interactions (Pi-stacking, Pi-alkyl), and the number of hydrophobic contacts was large (12 each), which also suggested that the ligands were highly complementary to the hydrophobic pocket of the protease. In contrast, remdesivir forms only two hydrogen bonds and two hydrophobic contacts but still has the strongest binding affinity, which may be attributed to supplementary polar and π–π aromatic interactions that increase the stability of the complex [42].

Table 4. Binding scores, number of chemical interactions, and types of interactions of MDG derivatives (**2**-**5**) and the standard drug remdesivir against SARS-CoV-2 RdRp (6M71).

Entry	SARS-CoV-2 RdRp (6M71)			
	Binding Affinity	**No. of Hydrogen Bond**	**No. of Hydrophobic Bond**	**Interaction type**
1	-5.4	4	0	H
2	-7.1	3	1	H, Pi
3	-6.4	4	12	H, C, PS, PA, A
4	-6.5	5	12	H, C, A, PA
5	-4.3	5	5	H, C, A, PA,
Remdesivir	-10.4	2	2	H, A, PA

H = conventional hydrogen bond; C = carbon–hydrogen bond; A= alkyl; PA = Pi–alkyl; PPS = Pi–Pi stacked; PS = Pi–sigma; PPT = Pi–Pi T-shaped.

Table 5 shows that compound **1** was stabilized by the formation of two hydrogen bonds with HIS816 (2.77 A) and one hydrophobic interaction with TYR831 (2.89 A). Among the screened compounds, compound **2**, with the best binding affinity (-7.1 kcal/mol), formed four hydrogen bonds with LYS47 and HIS133 and one hydrophobic contact with ALA130 (5.20 A) (Figure 7).

Table 5. Nonbonding interactions of MDG derivatives (**2**-**5**) with amino acid residues of 6M71.

Entry	SARS-CoV-2 RdRp (6M71)			
	Hydrogen Bond		Hydrophobic Bond	
	Residues	Distance (Å)	Residues	Distance (Å)
1	HIS816	2.76573		
	TYR831	2.88702		
2	LYS47	2.46489	ALA130	5.19625
	LYS47	2.92892		
	HIS133	2.41804		
	UNK1	2.33429		
	LYS47	2.98931		
3	SER255	2.70075	ARG249	4.30247
	ARG349	2.78491	PRO322	4.55439
	ARG349	2.71459	PRO461	3.90888
			TYR265	5.36775
			TYR265	5.15982
			TRP268	5.16777
4	SER709	2.86577	LYS47	5.35194
	LYS714	2.84287	LYS47	5.18321
	LYS714	2.78385	LYS47	5.35806
	GLY774	3.45743	ALA130	3.81853
	SER709	3.37508	LYS780	3.76378
			LYS780	5.26430
5	LYS27	2.6179	PRO178	4.19792
	LYS27	2.09342	LEU35	5.04209
	LYS27	1.96784	LEU122	4.89819
	TRP182	2.60541	TRP182	4.63657
	TRP182	3.37367		
Remdesivir	THR26	2.468	CYS145	5.166
	THR26	2.695	HIS163	4.137

Analysis of the docking poses indicated that several hydrogen-bonding and hydrophobic interactions stabilize the ligand–main protease (6M71) complexes, with notable variations in the number, distance, and type of interactions across the compounds.

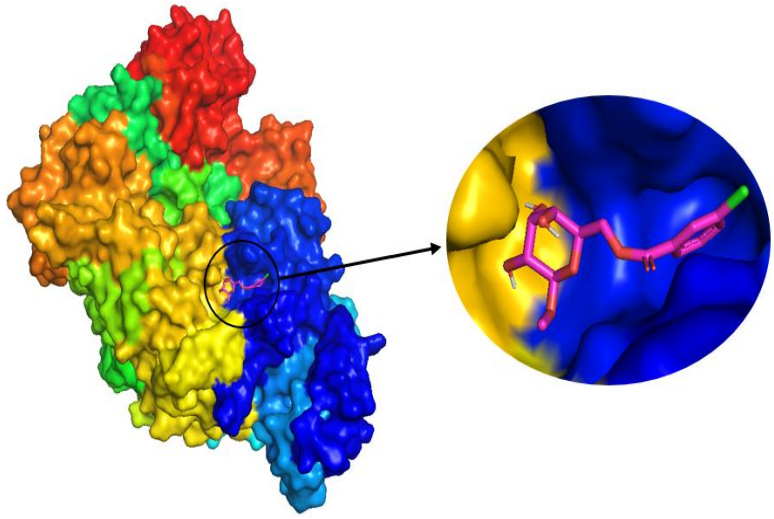

Figure 7. Docked pose of derivative (**2**) against 6M71 targeted protein.

The recurring nature of LYS47 is an indication that the residue is important for ligand anchoring in the active site of the protease. Compound **3** had an extensive interaction network, occupying SER255 and ARG349 with hydrogen bonds (~2.7 A) and several hydrophobic interactions with ARG249, PRO322, PRO461, TYR265, and TRP268 (3.9--5.4 A). Its binding energy (-6.4 kcal/mol) is probably due to the large number of nonpolar contacts it possesses. Notably, Compound **4** established a total of five hydrogen bonds with SER709, LYS714, and GLY774 and numerous hydrophobic contacts with LYS47, ALA130, and LYS780, which indicates a high degree of versatility in interactions and is in agreement with its stable docking score (-6.5 kcal/mol). Compound **5**, which had a lower affinity (-4.3 kcal/mol), only interacted with LYS27 and TRP182 via hydrogen bonds and moderately with PRO178, LEU35, and LEU122, and therefore did not have many interactions with the active pocket of the protease (Figure 8).

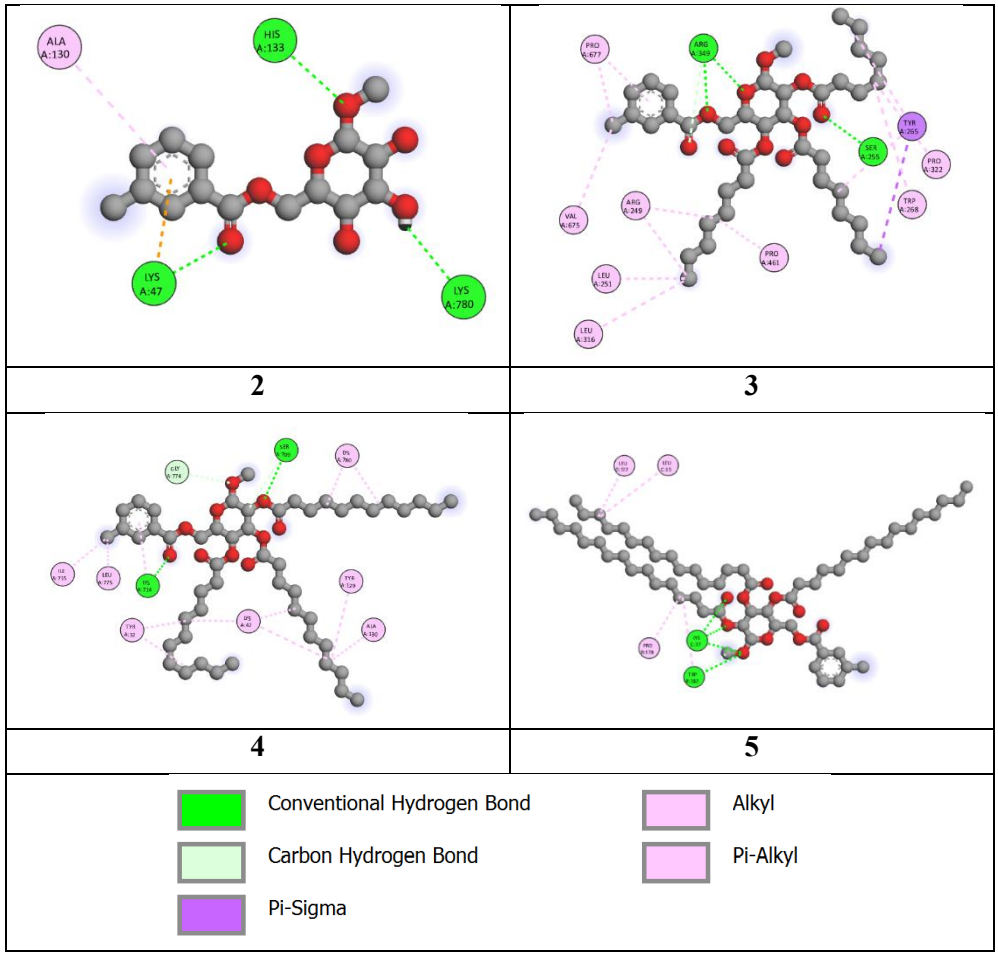

Figure 8. Nonbonding interactions of compounds (**2**, **3**, **4**, and **5**) in the binding pocket of 6M71.

In contrast, remdesivir, the reference ligand, had two hydrogen bonds with THR26 (2.47-2.70 A) and one hydrophobic interaction with CYS145 and HIS163 (4.14-5.17 A), residues that are also located in the main protease catalytic dyad region. This is why its binding affinity (-10.4 kcal/mol) is much greater and confirms the accuracy of docking. In general, the LYS47, ARG349, SER709, and THR26 residues are recurring binding hotspots in various ligands, highlighting their value in the process of protease-ligand recognition and inhibition [43]. The hydrogen-bond and

hydrophobic interaction surfaces of the selected potent compounds with the target proteins are shown in Figure 9.

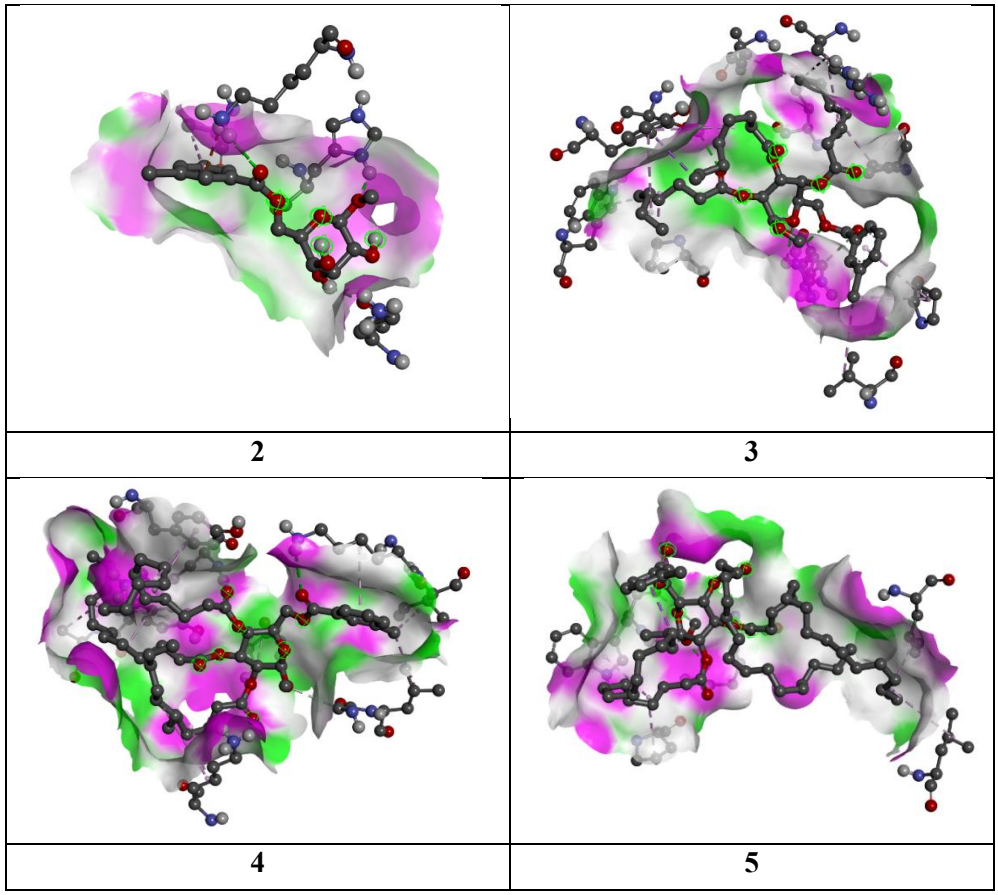

Figure 9. Hydrogen bonding & hydrophobic surface of 6M71 with **2, 3, 4,** and **5** compounds.

3.7 ADMET analysis

The SwissADME web tool was employed to evaluate the drug-likeness and physicochemical properties of the glucopyranoside derivatives [44]. The results are shown in Table 6, and the bioavailability radars are displayed in Figure 10. Using Lipinski's rule of five to look at oral bioavailability revealed a clear link between molecular size and compliance. The parent compound (**1**) and the minor derivative

(**2**) are both completely compliant, meaning that they meet all of the requirements and do not break any of them. They have the best molecular weight of 500 g/mol, acceptable LogP/w values (below 5), and good performance for hydrogen bond acceptors (HBAs) and donors (HBDs). Importantly, all three of the very active, large derivatives (**3**, **4**, and **5**) break the Lipinski rule twice. These breaches are due to their higher molecular complexity: all three have a molecular weight over the limit (711.32-1047.96 g/mol) and high lipophilicity, as shown by their high LogP/w values (4.77--8.50). Additionally, the high number of rotatable bonds (NRB) (up to 53 for compound **5**) and the increased total polar surface area (TPSA) are good for ensuring that the target binds to the right molecule, but they also suggest that the molecule is less flexible and may have trouble passing through cell membranes (Table 6). Molecular docking analyses suggest that these compounds represent strong lead candidates owing to their significant potency. However, the ADME results show that the largest derivatives will probably need to be given in ways other than orally or in ways that are specifically designed to achieve poor passive absorption.

Table 6. Lipinski's rule of five compliance and drug-likeness properties of the MDG (**1**) and its derivatives (**2-5**).

Entry	Mol. Wt.	HBA	HBD	logPo/w	NRB	TPSA	BA	Lipinski Rule	Violation
1	194.18	6	4	0.80	2	99.38	0.55	Yes	0
2	332.73	7	3	0.03	5	105.45	0.55	Yes	0
3	711.32	10	0	4.77	29	123.66	0.17	No	2
4	879.64	10	0	6.73	41	123.66	0.17	No	2
5	1047.96	10	0	8.50	53	123.66	0.17	No	2

Mol. Wt.: molecular weight; HBA: hydrogen bond acceptor; HDB: hydrogen bond donor; NRB: number of rotatable bonds; BA = bioavailability score; TPSA = total polar surface area

Figure 10 shows that the bioavailability data of the MDG derivatives (**2-5**) reflect the expected range of physicochemical parameters, with the pink zone indicating the area most suitable for oral bioavailability and the continuous red line representing the properties of the compounds.

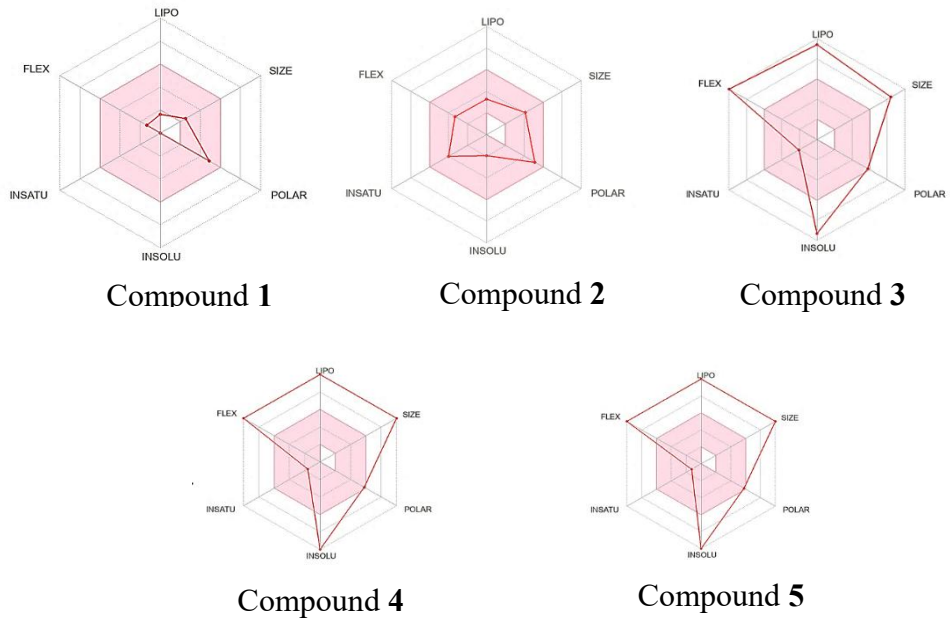

Figure 10. The bioavailability radar of the MDG (**1**) and its derivatives (**2-5**).

The initial safety profile of the glucopyranoside derivatives (**1-5**) was evaluated in silico *via* the ProTox-Tox 3.0 server to detect potential liabilities early in the drug discovery process, with the findings consolidated in Table 7. A very encouraging result is that all of the derivatives are consistently predicted to be inactive against both liver toxicity and nervous system toxicity. This often has high probability scores, which suggests that they have a good profile with respect to two common reasons for clinical attrition. Moreover, the compounds showed great expected profiles against genetic harm because they were all classed as inactive for both carcinogenicity and mutagenicity, which means that they are unlikely to interact with the genetic system. The analysis, however, highlights certain problems that need more research. All of the drugs were predicted to be active in both nephrotoxicity and cardiotoxicity testing, although the likelihood ratings were only moderate (between 0.64 and 0.75). Even with these warnings, the overall positive profile in important areas such as genotoxicity and organ-specific toxicity (liver/nerve) strongly supports moving the most active leads, especially compound **5**, to the next step of biological validation, where the predicted cardiotoxicity and nephrotoxicity must be carefully checked.

Table 7. Toxicity results were assessed through the ProTox-3.0 web server.

Classification	Target		Entry				
			1	**2**	**3**	**4**	**5**
Organ toxicity	Hepatotoxicity	Prediction	Inactive	Inactive	Inactive	Inactive	Inactive
		Probability	0.95	0.77	0.86	0.86	0.86
	Neurotoxicity	Prediction	Inactive	Inactive	Inactive	Inactive	Inactive
		Probability	0.93	0.89	0.78	0.78	0.78
	Nephrotoxicity	Prediction	Active	Active	Active	Active	Active
		Probability	0.75	0.55	0.64	0.64	0.64
	Cardiotoxicity	Prediction	Active	Active	Active	Active	Active
		Probability	0.95	0.67	0.71	0.71	0.71
Toxicity end points	Carcinogenicity	Prediction	Inactive	Inactive	Inactive	Inactive	Inactive
		Probability	0.86	0.76	0.59	0.59	0.59
	Immunotoxicity	Prediction	Inactive	Inactive	Active	Active	Active
		Probability	0.99	0.79	0.87	0.87	0.87
	Mutagenicity	Prediction	Inactive	Inactive	Inactive	Inactive	Inactive
		Probability	0.79	0.74	0.82	0.82	0.82
	Cytotoxicity	Prediction	Inactive	Inactive	Inactive	Inactive	Inactive
		Probability	0.86	0.65	0.75	0.75	0.75

4. Conclusion

This study employed a comprehensive computational approach, including DFT, quantum chemical descriptors, molecular docking, and ADMET analysis, to identify potent SARS-CoV-2 inhibitors on the basis of the MDG scaffold. DFT and FMO studies revealed that structural modifications, particularly the addition of long aliphatic and 3-chlorobenzoyl groups, significantly altered the electronic properties of MDG, reducing the HOMO–LUMO gap and thereby increasing its molecular softness and reactivity. Compound **5** emerged as the most promising inhibitor, displaying the lowest binding energies and key interactions such as pi–pi stacking and extensive hydrophobic contacts. ADMET predictions suggested favorable pharmacokinetic profiles, supporting their drug-likeness. Overall, these results highlight the MDG scaffold as a viable framework for SARS-CoV-2 inhibitor development, with compound **5** serving as a strong pharmacophore. Future work should focus on *in vitro* validation, lead optimization to reduce the molecular weight and lipophilicity, and exploration of formulation strategies to address potential bioavailability and safety challenges.

Acknowledgment

The authors gratefully acknowledge Berger Paints Bangladesh and the Ministry of Science and Technology (MoST), Bangladesh (Grant No. SRG-256652, 2025), for funding this work.

References

[1] Y. Kumar, H. Singh and C. N. Patel : Journal of Infection and Public Health, 2020, **13**, 1210–1223.

[2] N. Zhu, D. Zhang, W. Wang, X. Li, B. Yang, J. Song and et al. : New England Journal of Medicine, 2020, **382**, 727–733.

[3] D. S. Kolybalov, E. D. Kadtsyn and S. G. Arkhipov : Computation, 2024, **12**(1), 18.

[4] A. Khalili and M. Ahmad : International Journal of Molecular Sciences, 2015, **16**, 18149-18184.

[5] M. M. Islam, M . Arifuzzaman, M. M. Rahman, M. A. Rahman and S. M. A. Kawsar : Hacettepe Journal of Biology and Chemistry, 2019, **47**(2), 153-164.

[6] X. Cao, X. Du, H. Jiao, Q. An, R. Chen, P. Fang, J. Wang and B. Yu : Acta Pharmaceutica Sinica B, 2022, **12**, 3783-3821.

[7] M. Arifuzzaman, M. M. Islam, M. M. Rahman, M. A. Rahman and S. M. A. Kawsar : Acta Pharmaceutica Sciences, 2018, **56**(4), 7-22.

[8] O. Daoui, S. Elkhattabi and S. Chtita : Structural Chemistry, 2022, **33**, 1667-1690.

[9] J. H. Cummings, M. B. Roberfroid, H. Andersson, C. Barth, A. Ferro-Luzzi, Y. Ghoos, M. Gibney, K. Hermansen, W. P. T. James, O. Korver, D. Lairon, G. Pascal and A. G. S. Voragen : European Journal of Clinical Nutrition, 2010, **64**, 334-334.

[10] S. Chtita, S. Belaidi, F. A. Qais, M. Ouassaf, M. M. Almogren, A. A. Al-Zahrani, M. Bakhouch, A. Belhassan, H. Zaki, M. Bouachrine and T. Lakhlifi : Journal of King Saud University – Science, 2022, **34**, 102226.

[11] A. K. M. S. Kabir, S. M. A. Kawsar, M. M. R. Bhuiyan, M. S. Rahman and M. E. Chowdhury : Pakistan Journal of Scientific and Industrial Research, 2009, **52**(3), 138-142.

[12] A. K. M. S. Kabir, S. M. A. Kawsar, M. M. R. Bhuiyan, M. S. Rahman and B. Banu : Chittagong University Journal of Biological Sciences, 2008, **3**(1-2), 53-64.

[13] V. Judge, B. Narasimhan, M. Ahuja, D. Sriram, P. Yogeeswari, E. Clercq, C. Pannecouque and J. Balzarini : Medicinal Chemistry, 2013, **9**, 53-76.

[14] A. K. M. S. Kabir, S. M. A. Kawsar, M. M. R. Bhuiyan, M. R. Islam and M. S. Rahman : Bulletin of Pure & Applied Sciences, 2004, **23C**(2), 83-91.

[15] S. M. A. Kawsar, A. A. Hamida, A. U. Sheikh, M. K. Hossain, A. C. Shagir, A. F. M. Sanaullah, M. A. Manchur, H. Imtiaj, Y. Ogawa, Y. Fujii, Y. Koide and Y. Ozeki : International Journal of Organic Chemistry, 2015, **5**(4), 232-245.

[16] J. Wang, Y. Zhang, Q. Lu, D. Xing and R. Zhang : Frontiers in Pharmacology, 2021, **12**, 756724.

[17] S. M. A. Kawsar, R. Matsumoto, Y. Fujii, H. Yasumitsu, C. Dohgasaki, M. Hosono, K. Nitta, J. Hamako, T. Matsui, K. Noriaki and Y. Ozeki : Biochemistry, 2009, **74**(7), 709-716.

[18] S. M. A. Kawsar, R. Matsumoto, Y. Fujii, H. Matsuoka, N. Masuda, C. Iwahara, H. Yasumitsu, R. A. Kanaly, S. Sugawara, M. Hosono, K. Nitta, N. Ishizaki, C. Dogasaki, J. Hamako, T. Matsui and Y. Ozeki : Protein Journal, 2011, **30**(7), 509-519.

[19] S. M. A. Kawsar, G. Mostafa, E. Huq, N. Nahar and Y. Ozeki : International Journal of Biological Chemistry, 2009, **3**(1), 42-48.

[20] S. M. A. Kawsar, E. Huq and N. Nahar : International Journal of Pharmacology, 2008, **4**(4), 297–300.

[21] V. Mody, J. Ho, S. Wills, A. Mawri, L. Lawson, M. C. C. J. C. Ebert and et al. : Communications Biology, 2021, **4**, 93.

[22] D. Geedkar, A. Kumar and P. Sharma : Scientific Reports, 2024, **14**, 10419.

[23] M. Dutta, A. M. Tareq, A. Rakib, S. Mahmud, S. A. Sami, J. Mallick and et al. : Biology, 2021, **10**, 789-791.

[24] A. A. Rabaan, S. H. Al-Ahmed, M. A. Garout, A. M. Al-Qaaneh, A. A. Sule, R. Tirupathi and et al. : Pathogens, 2021, **10**, 534-536.

[25] L. Sun, D. R. Middleton, P. L. Wantuch, A. Ozdilek and F. Y. Avci : Glycobiology, 2016, **26**, 1029-1040.

[26] M. J. Frisch, G. W. Trucks, H. B. Schlegel, G. E. Scuseria, M. A. Robb, J. R. Cheeseman, G. Scalmani, V. Barone, B. Mennucci, G. A. Petersson, H. Nakatsuji, M. Caricato, X. Li, H. P. Hratchian, A. F. Izmaylov, J. Bloino, G. Zheng and J. L. Sonnenberg : Gaussian Software Documentation, 1999, **16**, 1134-1137.

[27] A. D. Becke : Physical Review A, 1988, **38**, 3098–3100.

[28] C. Lee, W. Yang and R. G. Parr : Physical Review B, 1988, **37**, 785–789.

[29] R. G. Pearson : Proceedings of the National Academy of Sciences, 1986, **83**, 8440-8441.

[30] Z. Jin, X. Du, Y. Xu, Y. Deng, M. Liu, Y. Zhao and et al. : Nature, 2020, **582**, 289-293.

[31] S. Dallakyan and A. J. Olson : Methods in Molecular Biology, 2015, 243-250.

[32] O. Trott and A. J. Olson : Journal of Computational Chemistry, 2009, **31**, 232-233.

[33] H. Yang, C. Lou, L. Sun and et al. : Bioinformatics, 2019, **35**(6), 1067-1069.

[34] C. A. Lipinski, F. Lombardo, B. W. Dominy and et al. : Advanced Drug Delivery Reviews, 2001, **46**(1-3), 3-26.

[35] J. Ferdous and S. M. A. Kawsar : Chittagong University Journal of Science, 2020, **42**(1), 58-83.

[36] S. M. A. Kawsar and M. Hosen : Turkish Computational and Theoretical Chemistry, 2020, **4**, 59-66.

[37] N. Bhattacharjee, J. A. Shakil, S. P. Saikat, M. R. Hossain, Prinsa, S. Saha and S. M. A. Kawsar : ChemistrySelect, 2025, **10**(30), 2470.

[38] M. A. Mumit, T. K. Pal, M. A. Alam, M. A-A-A. A. Islam, S. Paul and M. C. Sheikh : Journal of Molecular Structure, 2020, **1220**, 128715.

[39] R. G. Pearson : Proceedings of the National Academy of Sciences U.S.A., 1986, **83**, 8440–8441.

[40] A. A. Elfiky : Journal of Biomolecular Structure and Dynamics, 2021, **39**, 3204-3212.

[41] X. Liu and X-J. Wang : Journal of Genetics and Genomics, 2020, **47**(2), 119-121.

[42] D. B. D. Oliveira and A. C. Gaudio : Molecular Informatics, 2001, **19**(6), 599-601.

[43] E. R. Esharkawy, F. A. Almalki and T. BenHadda : Bioorganic Chemistry, 2022, **120**, 105587.

[44] M. Anowar Hosen, A. Alam, M. Islam, Y. Fujii, Y. Ozeki and S. M. A. Kawsar : Bulgarian Chemical Communications, 2021, **53**(3), 327-342.